Geophysical Research Letters

RESEARCH LETTER
10.1029/2024GL112399

Rapid Response of Martian Magnetotail to Solar Wind Disturbance: Tianwen-1 and MAVEN Joint Observations

Z. Z. Guo[1,2], H. S. Fu[1,2], J. B. Cao[1,2], Y. M. Wang[3,4], M. Ge[1,2], T. Y. Zhou[1,2], W. D. Fu[1,2], and Z. Wang[1,2]

[1]School of Space and Environment, Beihang University, Beijing, China, [2]Key Laboratory of Space Environment Monitoring and Information Processing, Ministry of Industry and Information Technology, Beijing, China, [3]Deep Space Exploration Laboratory/School of Earth and Space Sciences, University of Science and Technology of China, Hefei, China, [4]CAS Center for Excellence in Comparative Planetology/CAS Key Laboratory of Geospace Environment/Mengcheng National Geophysical Observatory, University of Science and Technology of China, Hefei, China

Key Points:

- We report for the first time the rapid response of Martian magnetotail to the solar wind (SW) disturbance by using Tianwen-1 and MAVEN data
- A 20% increase (or decrease) in P_{SW} and a 30° (or 50°) rotation of interplanetary magnetic field clock angle could cause the Martian magnetotail to swing
- These two SW disturbances could lead to oscillations of the Martian magnetotail

Correspondence to:
H. S. Fu,
huishanf@gmail.com

Citation:
Guo, Z. Z., Fu, H. S., Cao, J. B., Wang, Y. M., Ge, M., Zhou, T. Y., et al. (2024). Rapid response of Martian magnetotail to solar wind disturbance: Tianwen-1 and MAVEN joint observations. *Geophysical Research Letters*, *51*, e2024GL112399. https://doi.org/10.1029/2024GL112399

Received 10 SEP 2024
Accepted 27 NOV 2024

Abstract The Martian magnetotail is largely controlled by the solar wind (SW) and is modulated by variations in the upstream drivers. However, due to the limitations of single-spacecraft observations, the effects of SW variations on the Martian magnetotail have not been fully understood so far. Here, using Tianwen-1 and MAVEN data, we report for the first time the rapid response of Martian magnetotail to the SW disturbance. In our study, Tianwen-1 detected the flapping of Martian magnetotail, while MAVEN monitored disturbances in the upstream SW. The results indicate that a 20% increase (or decrease) in SW dynamic pressure and a 30° (or 50°) rotation of interplanetary magnetic field clock angle could cause the Martian magnetotail to swing rapidly. These two SW disturbances could lead to oscillations of the Martian magnetotail. This study reveals the importance of joint observations for studying the interaction between the SW and Mars.

Plain Language Summary Mars lacks an intrinsic global magnetic field and as a result solar wind (SW) interacts directly with its ionosphere and atmosphere, leading to a high dependence of the Martian induced magnetosphere on SW conditions. Understanding the interaction between the SW and Mars can provide critical information for studies of planetary evolution, especially the effect of the SW on the Martian magnetotail. In previous studies, using single satellite observations, we limit ourselves to studying some local physical processes or statistical properties. Here, based on the joint measurements by Tianwen-1 and MAVEN, we observed the rapid response of Martian magnetotail to the SW disturbance, finding that a 20% increase (or decrease) in SW dynamic pressure and a 30° (or 50°) rotation of IMF clock angle could cause the Martian magnetotail to swing rapidly. These two SW disturbances could lead to oscillations of the Martian magnetotail. These results can help us understand the SW interaction with the Martian induced magnetosphere.

1. Introduction

Mars is the farthest terrestrial planet from the sun in the inner solar system and one of the key targets for human deep space exploration. As we all know, Mars lacks a global dipole magnetic field powered by an active dynamo, but it retains localized and heterogeneous crustal magnetic fields (Acuña et al., 1999). This results in the solar wind (SW) being able to interact directly with the ionosphere and atmosphere of Mars, forming an induced magnetosphere (e.g., Nagy et al., 2004; Ramstad et al., 2020). A number of plasma boundaries and regions form in Martian induced magnetosphere, such as the bow shock (BS), the induced magnetosheath, the induced magnetopause, the magnetic pile-up region and the induced magnetotail (e.g., Bertucci et al., 2003; Crider et al., 2002; Lundin et al., 1991; Mazelle et al., 2004; Zhang et al., 1991). The induced magnetotail forms in the Martian wake region from interplanetary magnetic field (IMF) lines draped around the dayside ionosphere and stretched anti-sunward behind the Mars, consisting of two lobes, directed sunward and anti-sunward, separated by a cross-tail current sheet (e.g., Fedorov et al., 2006; Nagy et al., 2004). The orientation of the current sheet is determined primarily by the direction of the upstream IMF, which means that the Martian magnetotail is modulated by the upstream SW and becomes particularly active and sensitive (e.g., Ma et al., 2014; Romanelli et al., 2018, 2019).

The Martian magnetotail is a natural current sheet laboratory (e.g., Artemyev et al., 2017; Brain et al., 2007; Grigorenko et al., 2017, 2019; Guo et al., 2021, 2022), populated by a variety of field structures that facilitate the transport of mass, momentum, and energy through a series of processes, including magnetic reconnection (e.g., Halekas et al., 2009; Harada et al., 2015), magnetic structures evolution (e.g., DiBraccio et al., 2015; Hara

et al., 2017), and current sheet flapping (e.g., DiBraccio et al., 2017; Guo et al., 2022), etc. Such processes in space plasma have been proved to play important roles in energy conversion (e.g., Fu et al., 2011, 2012, 2013, 2017, 2019, 2020a, 2020b, 2020c; Cao et al., 2009, 2013; Z. Wang et al., 2019, 2020, 2024; Xu et al., 2018, 2021; Yu et al., 2022; Zhao et al., 2019). In Martian space environment, the data recorded by previous Mars exploration missions (Mars Global Surveyor, Mars Express, Mars Atmosphere and Volatile EvolutioN, etc) have enabled extensive investigations of the Martian magnetotail dynamics. Halekas et al. (2009) presented MGS measurements of reconnection Hall magnetic fields at current sheets on the nightside of Mars. Later, the process of magnetic reconnection in the near-Mars magnetotail was reported one after another by using MAVEN measurements and demonstrated to be effective in facilitating the escape of planetary heavy ions (e.g., Harada, Halekas, et al., 2017; Harada et al., 2015). Moreover, the flux rope produced by magnetic reconnection in the Martian tail current sheet could facilitate the burst escape of planetary ions (e.g., Hara et al., 2017). Besides, the cross-tail current sheet, filling with planetary ions, has been identified as a main ion escape channel at Mars. Since the $J \times B$ force due to the magnetic shear stresses of the draped field lines is the strongest in the center of tail, planetary ions could be accelerated to keV energies or more in the current sheet (e.g., Dubinin et al., 2011, 2012). In addition, the current sheet flapping, one of the most common phenomena of the magnetotail activity, can dramatically change the configuration of the magnetotail current sheet and release the stored field energy as wave motions (e.g., Artemyev et al., 2017; DiBraccio et al., 2017; Fedorov et al., 2006; Grigorenko et al., 2017, 2019). Thus, studying in the Martian magnetotail is important for understanding the planetary evolution.

However, the Martian magnetotail is highly dependent on the upstream SW conditions (e.g., DiBraccio et al., 2018; Xu et al., 2020), and the interaction between SW and the Martian magnetotail has not been fully understood due to the lack of multi-satellite cooperative observation. China's first successful planetary exploration (Wan et al., 2020), the Tianwen-1, arrived at Mars on 10 February 2021, along with the synchronous operation of the MAVEN, provides an opportunity to investigate the effect of the SW on the Martian induced magnetosphere. In this letter, we utilize synchronous measurements from Tianwen-1 and MAVEN to study the response of Martian magnetotail to the upstream SW disturbance.

2. Data and Observations

The data we used are from the Tianwen-1 (Wan et al., 2020) and MAVEN (Jakosky et al., 2015) missions. Among them, the Mars Orbiter Magnetometer (MOMAG; Liu et al., 2020; Y. Wang et al., 2023; G. Q. Wang et al., 2024; Zou et al., 2023) on board the Tianwen-1 orbiter is designed to measure the magnetic fields of and surrounding Mars. MOMAG will be operated at a sampling frequency of 32 Hz when the orbiter is both near the periareon (about 265 km from the surface) and near the apoareon (about 11,945.6 km). Throughout the rest of the orbit, MOMAG will be operated at a sampling frequency of 1 Hz. Each orbit is about 7.8 hr. In addition, the parameters of upstream SW are measured by MAVEN spacecraft, including magnetic field data from the Magnetometer (MAG; Connerney et al., 2015), ion data from the Solar Wind Ion Analyzer (SWIA; Halekas et al., 2015) and electron data from the Solar Wind Electron Analyzer (SWEA; Mitchell et al., 2016). All the data are presented in Mars Solar Orbital (MSO) coordinates unless otherwise specified. The X_{MSO} is directed from the center of the planet toward the center of the Sun, Y_{MSO} points opposite to the direction of Mars' orbital velocity component perpendicular to X_{MSO}, and Z_{MSO} completes the right-handed system.

The event of interest (the magnetotail flapping of Mars) was observed on 22 May 2022. Figure 1 presents an overview of this event during 12:38:00-13:38:00 UT from Tianwen-1 and MAVEN measurements. Figure 1a displays the magnetic field, Bx, By, Bz and |B|, observed by Tianwen-1/MOMAG in Martian magnetotail. Figures 1b–1e show the measurements of MAVEN for the same time period. More specially, Figure 1b is the magnetic field strength and three components, Figure 1c shows the three components of ion velocity, Figure 1d is the omnidirectional differential energy fluxes of electrons and Figure 1d is the ion spectrum. Based on the characteristics of the magnetic field and plasma, we are able to clearly identify the trajectory of the MAVEN. It passed through the BS from the induced magnetosheath (MS) into the SW, and then crossed the BS again into the MS (e.g., Cheng et al., 2023; Halekas et al., 2017), as shown in the bars above Figure 1b. Interestingly, Tianwen-1 detected multiple reversals of the magnetic field Bx component in Martian magnetotail during 13:00:00–13:25:00 UT (marked by the dashed box in Figure 1a). Usually, the reversal of Bx is considered as the main feature of the current sheet traversal process (e.g., DiBraccio et al., 2017; Grigorenko et al., 2017). In Martian magnetotail, the configuration of tail current sheet is responsive to the orientation of the upstream IMF and can change dramatically under varying upstream clock angles. Thus, it is common to detect multiple current sheet crossings on any

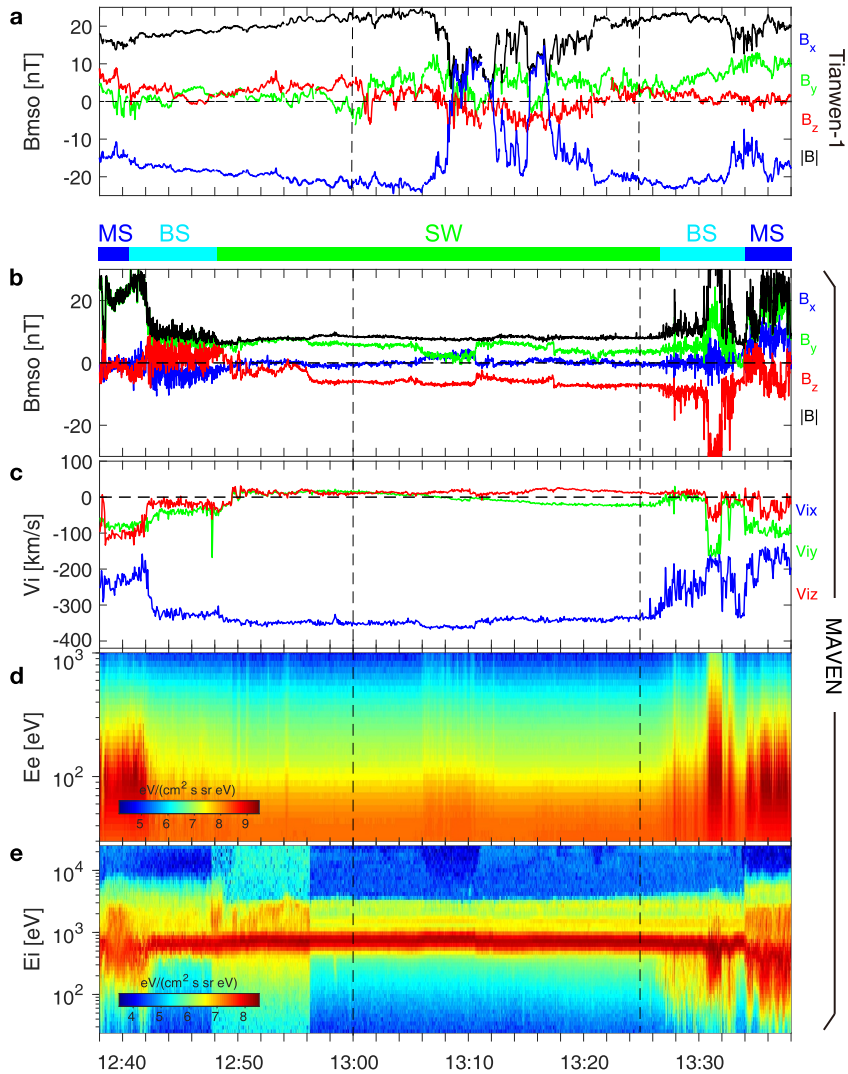

Figure 1. Long-term joint observations from 12:38:00 to 13:38:00 UT on 2022 May 22 by Tianwen-1 and MAVEN. (a) The magnetic field measured by Tianwen-1/MOMAG in the Martian distant magnetotail; (b) the magnetic field, (c) ion velocity, (d) electron spectrum and (e) ion spectrum observed by MAVEN. Mars Solar Orbital (MSO) represents the MSO coordinates. The X_{MSO} is directed from the center of the planet toward the center of the Sun, Y_{MSO} points opposite to the direction of Mars' orbital velocity component perpendicular to X_{MSO}, and Z_{MSO} completes the right-handed system. MS, magnetosheath; BS, bow shock; SW, solar wind.

given orbit as Tianwen-1 passes through the Martian magnetotail. These multiple crossing processes may be related to a variety of factors, including changes in the upstream IMF clock angle, reconnection of open magnetic fields, and the current sheet flapping due to the increase in the upstream SW dynamic pressure (e.g., DiBraccio et al., 2017; Luhmann et al., 2015). This means that multi-satellite joint observations (e.g., Harada, Gurnett, et al., 2017; Slavin et al., 2009) become important due to their ability to provide additional information on environment changes to these processes. We therefore further examined the measurements of MAVEN. During 13:00:00–13:25:00 UT, MAVNE was always located in the pristine SW (see the dashed box in Figures 1b–1e), meaning that it could simultaneously record disturbances in the upstream SW. A zoomed-in of this period is presented in Figure 2.

Detailed observations of the Martian magnetotail and simultaneously SW conditions are shown in Figure 2. From top to bottom, they are the positions of Tianwen-1 and MAVEN (Figures 2a–2c), the observations of By, Bz (Figure 2d), |B|, Bx (Figure 2e) in Martian magnetotail from Tianwen-1 MOMAG, as well as the SW magnetic field (Figure 2f), IMF clock angle (Figure 2g), density (Figure 2h), total velocity (Figure 2i) and dynamic pressure

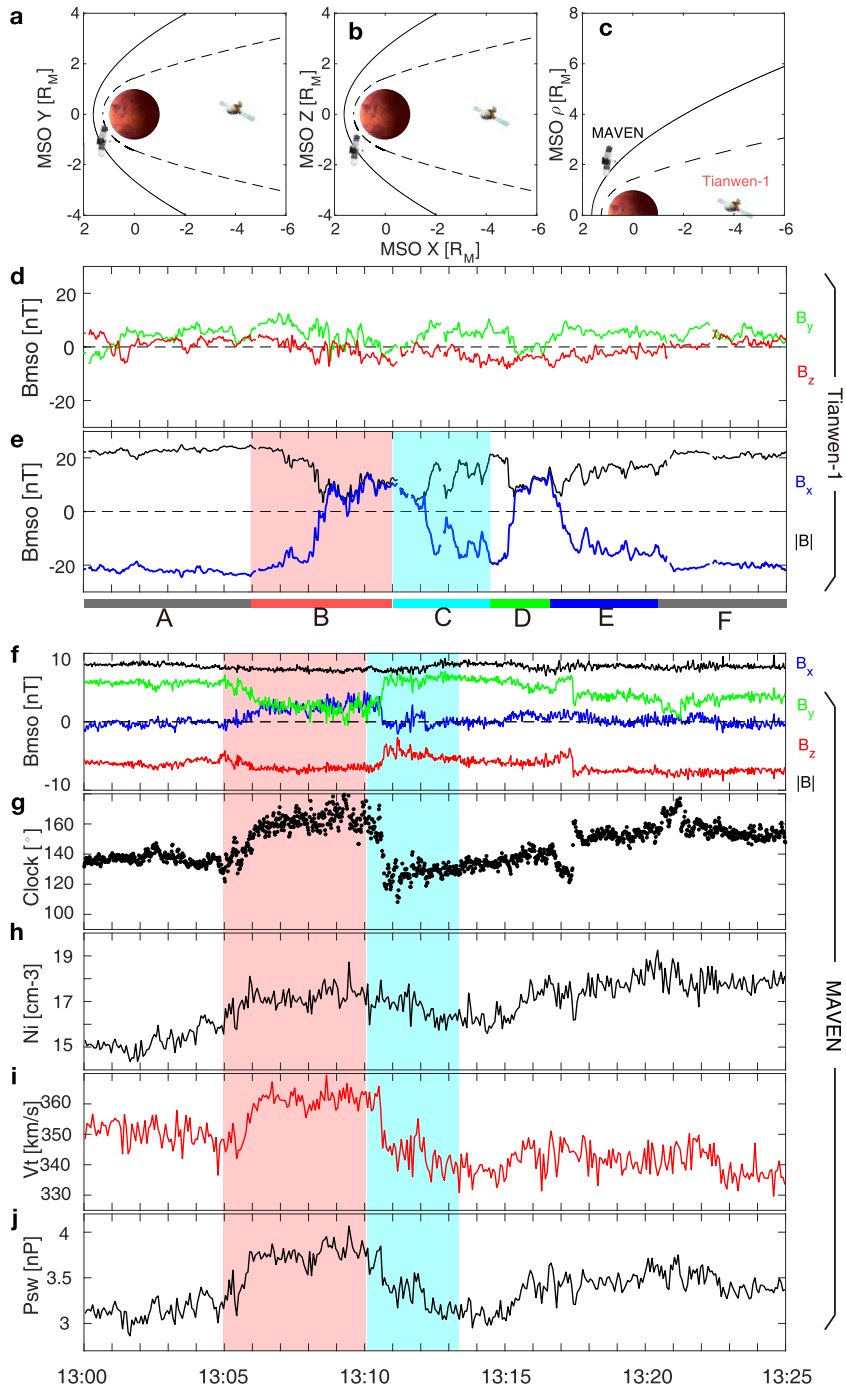

Figure 2. The response of Martian magnetotail to variations in upstream solar wind (SW) during 13:00:00–13:25:00 UT. The top row of panels shows the Tianwen-1 and MAVEN positions in panel (a) X_{MSO}−Y_{MSO} plane, (b) X_{MSO}−Z_{MSO} plane and (c) aberrated-MSO cylindrical coordinates, $\rho = \left(Y_{MSO}^2 + Z_{MSO}^2\right)^{0.5}$. The solid and dashed lines mark the bow shock and magnetic pileup boundary given by the model of Trotignon et al. (2006), respectively. (d) The By and Bz components, and (e) |B| and Bx observed by Tianwen-1. (f) The interplanetary magnetic field (IMF), (g) IMF clock angle, SW (h) density, (i) velocity and (j) dynamic pressure.

(Figure 2j) from MAVEN. From 13:00:00 to 13:25:00 UT, MAVEN was located around [1.1 −1.2 −1.3] R_M in MSO coordinates, within the SW; Tianwen-1 was located in the distant magnetotail, near [−4.1 0.2 0.3] R_M (R_M is Martian radii) in MSO coordinate (see Figures 2a–2c). In the Martian magnetotail, there was no significant

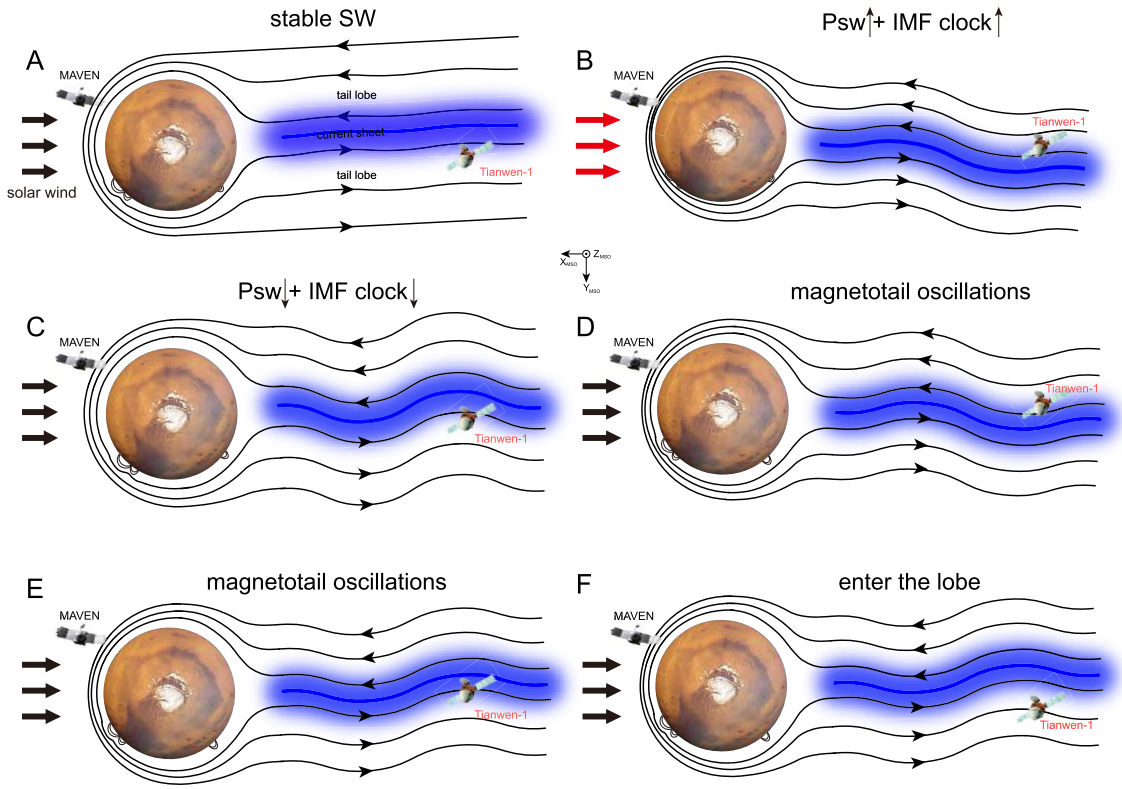

Figure 3. Schematic illustrations of the effects of solar wind (SW) disturbances on the Martian magnetotail. (A–F) Correspond to the state of the Martian magnetotail at time periods (A–F) above Figure 2f, respectively. (A) Calm state (B) and (C) the disturbances in SW dynamic pressure and interplanetary magnetic field (IMF) clock angel; (D, E) the oscillations of the magnetotail; (F) Tianwen-1 entered the dusk side lobe from the tail current sheet. The arrows in front of Mars indicate the SW disturbances. The blue areas denote the tail current sheet. All views are shown in the $X_{MSO}-Y_{MSO}$ plane. The raised curves on Mars indicate magnetic anomalies. SW, solar wind; P_{SW}, solar wind dynamic pressure; IMF clock, interplanetary magnetic field clock angle.

change in By and Bz components during such time period (see Figure 2d). From 13:00:00 to 13:05:56 UT (A-time period), Tianwen-1 observed a stable magnetic field, which was dominated by -Bx component and had a total field magnitude of about 20 nT (see Figure 2e), implying that the Tianwen-1 was located in the lobe. Before 13:05:00 UT, the upstream SW was also stable (see Figure 2f), and the IMF was mainly in +Y and −Z direction in MSO coordinate, indicating that the draped magnetic field lines should have positive Bx component on the dawn side magnetotail. And considering the negative Bx component observed by Tianwen-1, we can infer that Tianwen-1 should be located on the dusk side lobe, as shown in Figure 3A. From 13:05:56 to 13:11:00 UT, Tianwen-1 observed a gradual decrease in the Bx component from −20 nT, followed by a reversal, and then a gradual increase to 13 nT. The first reversal of tail Bx, marked by the pink shaded area in Figure 2e, corresponds to the B-time period. Interestingly, MAVEN monitored the SW disturbances about a minute ago, highlighted with pink shaded area in Figures 2f–2j (the first disturbance of SW). Firstly, it can be seen that the IMF clock angle gradually changes from ∼140° to ∼170°, a rotation of about 30° (see Figure 2g). What's more, the SW density gradually increases from 16 to 17.5 cm^{-3} (see Figure 2h), the total velocity rises from 350 km/s to 365 km/s (see Figure 2i), and the SW dynamic pressure (P_{SW}) increases from 3.1 to 3.8 nPa (see Figure 2j). The P_{SW} was calculated with mnV^2, where m is the mass of particle, n is the density, and the V is the velocity. These SW densities and dynamic pressures are relatively high compared to nominal conditions (Halekas et al., 2017). By combining the observations from Tianwen-1 and MAVEN, we infer that the changes in P_{SW} and the rotation of the IMF clock angle may result in the flapping of the Martian magnetotail, leading Tianwen-1 to enter the dawn side of current sheet from dusk side lobe, as shown in Figure 3B. Thus, Tianwen-1 observed the Bx component change from −20 to 13 nT. Here, we do not consider the reversal of Bx as the normal tail current sheet crossing process, and the relevant clarification will be provided below.

Subsequently, from 13:11:00–13:14:30 UT (the second reversal of tail Bx, marked by the cyan shaded area in Figure 2e, C-time period), Tianwen-1 observed that the tail Bx gradually changed from 13 nT to −17 nT.

Similarly, we continue to analyze the SW conditions. From 13:10:05 to 13:13:20 UT (marked by the cyan shaded area in Figures 2f–2j), the second disturbances of the SW were also very noticeable. The IMF clock angle rapidly rotated from about 170° to around 120° between 13:10:05 and 13:11:00 UT (see Figure 2g), and then gradually stabilized at around 120° between 13:11:00 and 13:13:20 UT. In addition, the P_{SW} gradually weakened (from 3.8 to 3 nPa) due to the reduced SW density and flow velocity during 13:10:05 to 13:13:20 UT (see Figures 2h–2j). These results may indicate that the second disturbances in the IMF clock angle and P_{SW} once again caused the swinging of the Martian magnetotail. Such process leads Tianwen-1 to pass from the dawn side of current sheet through its center to the dusk side of current sheet, which explains the second reversal of Bx observed by Tianwen-1 (C-time period in Figure 2e), as shown in Figure 3C.

And then, from 13:14:30 to 13:16:38 UT (D-time period in Figure 2e), the Tianwen-1 observed the third reversal of tail Bx from 14 nT to −15 nT. However, the IMF clock angle and P_{SW} are stable before this reversal of Bx, with clock angle ∼130° and Psw ∼3 nPa (from 13:12:30 to 13:14:30 UT, please see Figures 2g and 2j). We also noticed that the P_{SW} gradually strengthens (from 3 to 3.5 nPa, see Figure 2j) during the D-time period. But this increase in P_{SW} should not be the reason for the third reversal of tail Bx, as they occurred almost simultaneously. This indicates that the third reversal of Bx should not be caused by the SW. Combined with the analysis of the first two swings of the magnetotail, the third reversal of Bx could result from magnetotail oscillations triggered by the first and second SW disturbances. Similarly, from 13:16:38 to 13:20:20 UT (marked by blue bar below Figure 2f, E-time period), Tianwen-1 observed the fourth reversal of tail Bx from 14 nT to −15 nT. Before the fourth reversal of tail Bx, the IMF angle is stable at about 140°, and the Psw change is vague due to strong fluctuations in the particle moments (see Figures 2h and 2i). We speculate that the fourth reversal of Bx could be also the result of magnetotail oscillations. In other words, the tail flapping during periods D and E could result from lingering oscillations triggered by the first and second upstream SW disturbances, leading Tianwen-1 on the dusk side current sheet to enter the dawn side current sheet (as shown in Figure 3D) and then return to the dusk side (as shown in Figure 3E). Afterwords, Tianwen-1 detected that Bx changed from −15 nT to −20 nT and then remained the lobe level during 13:20:20–13:25:00 UT (F-time period in Figure 2e), indicating that the Tianwen-1 entered the dusk side lobe from the dusk side current sheet, as shown in Figure 3F. Before Tianwen-1 entered the lobe, the IMF clock angle was stable at about 150°, but the change in P_{SW} was also vague due to fluctuations of particle moments (Figures 2g–2j). Therefore, it is uncertain whether the process of Tianwen-1 entering the lobe is affected by the SW, but this is not the focus of our attention.

3. Discussion

In our event, several details are worth discussing and clarifying. First of all, the rapid response of the Martian magnetotail to variations in the upstream SW. Here we discuss the two clearest time periods, B-time and C-time periods in Figure 2e. For the first reversal of Bx (see the pink shaded area in Figure 2), the IMF clock angle and P_{SW} started to increase at 13:05:00 UT, while the Bx observed by Tianwen-1 began to decrease at 13:05:56 UT, with a time difference of 56 s. Likewise, for the second reversal of Bx (see cyan shaded area in Figure 2), the IMF clock angle and P_{SW} began to decrease from 13:10:05 UT; however, the Bx started to decrease at 13:11:00 UT, with a 55-s time difference. Based on the distance between Tianwen-1 and MAVEN along the X_{MSO}-axis (∼5.2 R_M) and the SW velocity (Vx∼350 km/s), we estimated the time scale between the two satellites to be approximately 50 s, consistent with the time lags of the swinging of the Martian magnetotail. Therefore, the first and second reversals of the tail Bx component should be directly caused by upstream SW disturbances. It is worth mentioning that previous simulation study (Romanelli et al., 2018) reported the effect of IMF rotation on the Martian magnetosphere and estimated the response timescale of magnetotail to IMF rotation to be about a few minutes; and they focused mainly on the disturbance of the IMF. Here, the disturbances in IMF clock angle and P_{SW} are very clear in our event (B-time and C-time periods), and the response time of the magnetotail is close to the propagation time of the SW flow. In general, the propagation speed of the P_{SW} pulse is closed to the Alfvén speed or the fast magnetosonic speed (e.g., Harada, Gurnett, et al., 2017), and it may take several minutes for the pulse to propagate from upstream to the Martian magnetotail. However, the change of the P_{SW} (∼20%) in our event may not be sufficient to generate a dynamic pressure pulse. Although the magnetotail flapping is related to the variations in upstream IMF clock angle and P_{SW}, it may not be attributed to dynamic pressure pulse, and the corresponding physical mechanism may need to be further discussed in future simulation work. What's more, we can quantify the lag times of the current sheet flapping motions (the reversals of tail Bx) to the first two SW disturbances by cross-correlation analysis. Based on the time-series data of tail Bx component from Tianwen-1

and clock angle from MAVEN during the pink-shaded and cyan-shaded periods in Figure 2, we estimated the lag times of the first two current sheet flapping motions to upstream SW disturbances to be about 205 s (corresponding to maximum correlation coefficient of 0.65) and 130 s (corresponding to maximum correlation coefficient of 0.73), respectively.

Additionally, the reversals of Bx observed by Tianwen-1 above were identified as the result of the Martian magnetotail wobbles, rather than Tianwen-1 traversing the tail current sheet normally (from one lobe to the other), which may require more clarifications. To analyze Tianwen-1's trajectory in the normal direction of the cross-tail current sheet, we converted its position into the Mars-Sun-Electric field (MSE) frame. In the MSE frame, X_{MSE} is antiparallel to the SW flow vector ($-V_{SW}$), Z_{MSE} defines the orientation of the SW motional electric field ($-V_{SW} \times B_{IMF}$), and Y_{MSE} completes this right-handed system. The normal direction of the current sheet formed by the draped magnetic field in the far magnetotail of Mars is usually parallel to the Y_{MSE} direction. If the current sheet is calm, the movement distance of the spacecraft in the Y_{MSE} direction should be close to its thickness while crossing the current sheet normally. Using upstream magnetic field and velocity measured by MAVEN, we convert the trajectory of Tianwen-1 to the corresponding MSE frame. During the first reversal of tail Bx, we used the average SW parameters from 13:06:00 to 13:10:00 UT to calculate the MSE coordinates and found that the Tianwen-1 moved approximately 272 km (from −0.19 to −0.11 R_M) in the Y_{MSE} direction. Similarly, we estimated that the Tianwen-1 moved about 340 km (from 0.13 to 0.23 R_M) in the Y_{MSE} direction during the multiple reversals of Bx (from 13:11:00 to 13:17:00 UT). These distances are slightly lower than the thickness of the cross-tail current sheet (e.g., Halekas et al., 2010; Riedler et al., 1991; Yeroshenko et al., 1990), ruling out the possibility of normal crossing tail current sheet. Therefore, it should be reasonable here to understand the multiple reversals of Bx observed by Tianwen-1 as the flapping of the magnetotail. We noticed that the spacecraft moved from negative Y_{MSE} to positive Y_{MSE} during the period from 13:10:00 to 13:11:00 UT. Generally, upstream IMF rotation could cause the MSE frame to rotate about the X_{MSE}-axis, which could result in the spacecraft moving from one side of the current sheet to the other, loading the satellite to observe the reversal of tail Bx component. However, the IMF rotation was accompanied by the change in P_{SW} in our event. Thus, we cannot identify which specific disturbance (IMF rotation or the change in P_{SW} or their combination) drives the reversal of tail Bx here. The onefold IMF rotation or variation in P_{SW} could also drive changes in the Martian magnetotail, and these observational evidences require further attention in our future work.

In previous study (e.g., DiBraccio et al., 2018), the Martian magnetotail lobes exhibit an angle twist, either clockwise or counterclockwise from the ecliptic plane. And the cross-tail current sheet is rotated away from the expected location for the induced magnetotail, resulting in a very complex configuration of Martian magnetotail. Thus, the kink-like configuration of cross-tail current sheet caused by twist tail may be present in the Martian magnetotail, and multiple reversals of tail Bx may also be observed as the spacecraft passes through it many times. But in our event, the Tianwen-1 moved a smaller distance than the thickness of the cross-tail current sheet during many reversals of tail Bx. Therefore, the explanation for the tail Bx reversals is more inclined to the current sheet flapping.

4. Conclusion

In this letter, based on the joint observations of Tianwen-1 and MAVEN, we report for the first time the rapid response of Martian magnetotail to the upstream SW disturbances. In our event, Tianwen-1 was located in the Martian distant magnetotail, while MAVEN stayed in the upstream SW. We can establish direct connections between the magnetotail flapping and the SW disturbances. Their observations indicate that a 20% increase in the P_{SW} and a 30° rotation of the IMF clock angle could lead to a rapid swing of the Martian magnetotail, causing Tianwen-1 to move from the dusk side lobe into the dawn side of current sheet. Subsequently, the second disturbances of the SW—a 20% decrease in the P_{SW} and a 50° rotation of the IMF clock angle, cause the Martian magnetotail to swing in the opposite direction of the first, leading Tianwen-1 to move from the dawn side of current sheet to its dusk side. The two SW disturbances may cause the lingering oscillations of the magnetotail, resulting in Tianwen-1 observing the third and fourth reversals of tail Bx component in the Martian magnetotail.

Data Availability Statement

The MOMAG data is from the Tianwen-1 mission. The MOMAG data used in this paper can be found in "HX1-Or_GRAS_MOMAG-DB-1 Hz_SCI_P_20220522122407_20220522192659_01218_B.2 C" file at the Lunar and Planetary Data Release System (https://moon.bao.ac.cn/web/enmanager/kxsj?missionName=HX1&zhN274ame=MOMAG&gradg=2C). The MOMAG data here could also be retrieved from the official site of the MOMAG team (http://space.ustc.edu.cn/dreams/tw1_momag/). All MAVEN data used in this study are available through the MAVEN Science Data Center (https://lasp.colorado.edu/maven/sdc/public/data/sci/).

Acknowledgments
We would like to thank the Tianwen-1 and MAVEN team for providing data access and support. Special thanks to J. E. P. Connerney, D. L. Mitchell and J. S. Halekas for their contributions in making available data from MAG, SWEA, and SWIA, respectively. This work was supported by NSFC Grants 42125403, 42241113, and "the Fundamental Research Funds for the Central Universities." We express our gratitude to the ISSI-BJ travel Grant for team "Understanding Electron-Scale Magnetic Structures in Space Plasmas" led by Elena Grigorenko and Huishan Fu. The calibration of MOMAG data is supported by NSFC 42130204.

References

Acuña, M., Connerney, J., Ness, N. F., Lin, R. P., Mitchell, D., Carlson, C. W., et al. (1999). Global distribution of crustal magnetization discovered by the Mars global surveyor AG/ER experiment. *Science*, *284*(5415), 790–793. https://doi.org/10.1126/science.284.5415.790

Artemyev, A. V., Angelopoulos, V., Halekas, J. S., Runov, A., Zelenyi, L. M., & McFadden, J. P. (2017). Mars's magnetotail: Nature's current sheet laboratory. *Journal of Geophysical Research: Space Physics*, *122*(5), 5404–5417. https://doi.org/10.1002/2017JA024078

Bertucci, C., Mazelle, C., Crider, D. H., Vignes, D., Acuña, M. H., Mitchell, D. L., et al. (2003). Magnetic field draping enhancement at the Martian magnetic pileup boundary from Mars global surveyor observations. *Geophysical Research Letters*, *30*(2), 1099. https://doi.org/10.1029/2002GL015713

Brain, D. A., Lillis, R. J., Mitchell, D. L., Halekas, J. S., & Lin, R. P. (2007). Electron pitch angle distributions as indicators of magnetic field topology near Mars. *Journal of Geophysical Research*, *112*(A9), A09201. https://doi.org/10.1029/2007JA012435

Cao, J. B., Fu, H. S., Zhang, T. L., Reme, H., Dandouras, I., & Lucek, E. (2009). Direct evidence of solar wind deceleration in the foreshock of the Earth. *Journal of Geophysical Research*, *114*(A2), A02207. https://doi.org/10.1029/2008JA013524

Cao, J. B., Wei, X. H., Duan, A. Y., Fu, H. S., Zhang, T. L., Reme, H., & Dandouras, I. (2013). Slow magnetosonic waves detected in reconnection diffusion region in the Earth's magnetotail. *Journal of Geophysical Research: Space Physics*, *118*(4), 1659–1666. https://doi.org/10.1002/jgra.50246

Cheng, L., Lillis, R., Wang, Y., Mittelholz, A., Xu, S., Mitchell, D. L., et al. (2023). Martian bow shock oscillations driven by solar wind variations: Simultaneous observations from Tianwen-1 and MAVEN. *Geophysical Research Letters*, *50*(16), e2023GL104769. https://doi.org/10.1029/2023GL104769

Connerney, J. E. P., Espley, J., Lawton, P., Murphy, S., Odom, J., Oliversen, R., & Sheppard, D. (2015). The MAVEN magnetic field investigation. *Space Science Reviews*, *195*(1–4), 257–291. https://doi.org/10.1007/s11214-015-0169-4

Crider, D. H., Acuña, M. S., Connerney, J. E. P., Vignes, D., Ness, N. F., Krymskii, A. M., et al. (2002). Observations of the latitude dependence of the location of the Martian magnetic pileup boundary. *Geophysical Research Letters*, *29*(8), 11–114. https://doi.org/10.1029/2001GL013860

DiBraccio, G. A., Dann, J., Espley, J. R., Gruesbeck, J. R., Soobiah, Y., Connerney, J. E. P., et al. (2017). MAVEN observations of tail current sheet flapping at Mars. *Journal of Geophysical Research: Space Physics*, *122*(4), 4308–4324. https://doi.org/10.1002/2016JA023488

DiBraccio, G. A., Espley, J. R., Gruesbeck, J. R., Connerney, J. E. P., Brain, D. A., Halekas, J. S., et al. (2015). Magnetotail dynamics at Mars: Initial MAVEN observations. *Geophysical Research Letters*, *42*(21), 8828–8837. https://doi.org/10.1002/2015GL065248

DiBraccio, G. A., Luhmann, J. G., Curry, S. M., Espley, J. R., Xu, S., Mitchell, D. L., et al. (2018). The twisted configuration of the Martian magnetotail: MAVEN observations. *Geophysical Research Letters*, *45*(10), 4559–4568. https://doi.org/10.1029/2018GL077251

Dubinin, E., Fraenz, M., Fedorov, A., Lundin, R., Edberg, N., Duru, F., & Vaisberg, O. (2011). Ion energization and escape on Mars and Venus. *Space Science Reviews*, *162*(1–4), 173–211. https://doi.org/10.1007/s11214-011-9831-7

Dubinin, E., Fraenz, M., Woch, J., Zhang, T. L., Wei, J., Fedorov, A., et al. (2012). Bursty escape fluxes in plasma sheets of Mars and Venus. *Geophysical Research Letters*, *39*(1), L01104. https://doi.org/10.1029/2011GL049883

Fedorov, A., Budnik, E., Sauvaud, J. A., Mazelle, C., Barabash, S., Lundin, R., et al. (2006). Structure of the Martian wake. *Icarus*, *182*(2), 329–336. https://doi.org/10.1016/j.icarus.2005.09.021

Fu, H. S., Chen, F., Chen, Z. Z., Xu, Y., Wang, Z., Liu, Y. Y., et al. (2020b). First measurements of electrons and waves inside an electrostatic solitary wave. *Physical Review Letters*, *124*(9), 095101. https://doi.org/10.1103/PhysRevLett.124.095101

Fu, H. S., Grigorenko, E. E., Gabrielse, C., Liu, C., Lu, S., Hwang, K.-J., et al. (2020a). Magnetotail dipolarization fronts and particle acceleration: A review. *Sci. China Earth Sci.*, *63*(2), 235–256. https://doi.org/10.1007/s11430-019-9551-y

Fu, H. S., Khotyaintsev, Y. V., André, M., & Vaivads, A. (2011). Fermi and betatron acceleration of suprathermal electrons behind dipolarization fronts. *Geophysical Research Letters*, *38*(16), L16104. https://doi.org/10.1029/2011GL048528

Fu, H. S., Khotyaintsev, Y. V., Vaivads, A., André, M., Sergeev, V. A., Huang, S. Y., et al. (2012). Pitch angle distribution of suprathermal electrons behind dipolarization fronts: A statistical overview. *Journal of Geophysical Research*, *117*(A12), A12221. https://doi.org/10.1029/2012JA018141

Fu, H. S., Khotyaintsev, Y. V., Vaivads, A., Retinò, A., & André, M. (2013). Energetic electron acceleration by unsteady magnetic reconnection. *Nature Physics*, *9*(7), 426–430. https://doi.org/10.1038/NPHYS2664

Fu, H. S., Vaivads, A., Khotyaintsev, Y. V., André, M., Cao, J. B., Olshevsky, V., et al. (2017). Intermittent energy dissipation by turbulent reconnection. *Geophysical Research Letters*, *44*(1), 37–43. https://doi.org/10.1002/2016GL071787

Fu, H. S., Xu, Y., Vaivads, A., & Khotyaintsev, Y. V. (2019). Super-efficient electron acceleration by an isolated magnetic reconnection. *The Astrophysical Journal Letters*, *870*(2), L22. https://doi.org/10.3847/2041-8213/aafa75

Fu, H. S., Zhao, M. J., Yu, Y., & Wang, Z. (2020c). A new theory for energetic electron generation behind dipolarization front. *Geophysical Research Letters*, *47*(6), e2019GL086790. https://doi.org/10.1029/2019GL086790

Grigorenko, E. E., Shuvalov, S. D., Malova, H. V., Dubinin, E., Popov, V. Y., Zelenyi, L. M., et al. (2017). Imprints of quasi-adiabatic ion dynamics on the current sheet structures observed in the Martian magnetotail by MAVEN. *Journal of Geophysical Research: Space Physics*, *122*(10), 176–193. https://doi.org/10.1002/2017JA024216

Grigorenko, E. E., Zelenyi, L. M., DiBraccio, G., Ermakov, V. N., Shuvalov, S. D., Malova, H. V., et al. (2019). Thin current sheets of sub-ion scales observed by MAVEN in the Martian magnetotail. *Geophysical Research Letters*, *46*(12), 6214–6222. https://doi.org/10.1029/2019GL082709

Guo, Z. Z., Fu, H. S., Cao, J. B., Fan, K., Yao, Z. H., Liu, Y. Y., et al. (2021). Betatron cooling of electrons in Martian magnetotail. *Geophysical Research Letters*, *48*(13), e2021GL093826. https://doi.org/10.1029/2021GL093826

Guo, Z. Z., Liu, Y. Y., Fu, H. S., Cao, J. B., Xu, Y., Wang, Z., et al. (2022). First observation of lower hybrid drift waves at the edge of the current sheet in the Martian magnetotail. *The Astrophysical Journal*, *933*(2), 128. https://doi.org/10.3847/1538-4357/ac722b

Halekas, J. S., & Brain, D. A. (2010). Global distribution, structure, and solar wind control of low altitude current sheets at Mars. *Icarus*, *206*(1), 64–73. https://doi.org/10.1016/j.icarus.2008.12.032

Halekas, J. S., Eastwood, J. P., Brain, D. A., Phan, T. D., Øieroset, M., & Lin, R. P. (2009). In situ observations of reconnection Hall magnetic fields at Mars: Evidence for ion diffusion region encounters. *Journal of Geophysical Research*, *114*(A11), A11204. https://doi.org/10.1029/2009JA014544

Halekas, J. S., Ruhunusiri, S., Harada, Y., Collinson, G., Mitchell, D. L., Mazelle, C., et al. (2017). Structure, dynamics, and seasonal variability of the mars-solar wind interaction: MAVEN solar wind ion analyzer in-flight performance and science results. *Journal of Geophysical Research: Space Physics*, *122*(1), 547–578. https://doi.org/10.1002/2016JA023167

Halekas, J. S., Taylor, E. R., Dalton, G., Johnson, G., Curtis, D. W., McFadden, J. P., et al. (2015). The solar wind ion analyzer for MAVEN. *Space Science Reviews*, *195*(1), 125–151. https://doi.org/10.1007/s11214-013-0029-z

Hara, T., Harada, Y., Mitchell, D. L., DiBraccio, G. A., Espley, J. R., Brain, D. A., et al. (2017). On the origins of magnetic flux ropes in near-Mars magnetotail current sheets. *Geophysical Research Letters*, *44*(15), 7653–7662. https://doi.org/10.1002/2017GL073754

Harada, Y., Gurnett, D. A., Kopf, A. J., Halekas, J. S., Ruhunusiri, S., Lee, C. O., et al. (2017). Dynamic response of the Martian ionosphere to an interplanetary shock: Mars express and MAVEN observations. *Geophysical Research Letters*, *44*(18), 9116–9123. https://doi.org/10.1002/2017GL074897

Harada, Y., Halekas, J. S., McFadden, J. P., Espley, J., DiBraccio, G. A., Mitchell, D. L., et al. (2017). Survey of magnetic reconnection signatures in the Martian magnetotail with MAVEN. *Journal of Geophysical Research: Space Physics*, *122*(5), 5114–5131. https://doi.org/10.1002/2017JA023952

Harada, Y., Halekas, J. S., McFadden, J. P., Mitchell, D. L., Mazelle, C., Connerney, J. E. P., et al. (2015). Magnetic reconnection in the near-Mars magnetotail: MAVEN observations. *Geophysical Research Letters*, *42*(21), 8838–8845. https://doi.org/10.1002/2015GL065004

Jakosky, B. M., Lin, R. P., Grebowsky, J. M., Luhmann, J. G., Mitchell, D. F., Beutelschies, G., et al. (2015). The Mars Atmosphere and Volatile Evolution (MAVEN) mission. *Space Science Reviews*, *195*(1–4), 3–48. https://doi.org/10.1007/s11214-015-0139-x

Liu, K., Hao, X. J., Li, Y. R., Zhang, T. L., Pan, Z. H., Chen, M. M., et al. (2020). Mars orbiter magnetometer of China's first Mars mission Tianwen-1. *Earth and Planetary Physics*, *4*(4), 384–389. https://doi.org/10.26464/epp2020058

Luhmann, J. G., Dong, C., Ma, Y., Curry, S. M., Mitchell, D., Espley, J., et al. (2015). Implications of MAVEN Mars near-wake measurements and models. *Geophysical Research Letters*, *42*(21), 9087–9094. https://doi.org/10.1002/2015GL066122

Lundin, R., Dubinin, E. M., Koskinen, H., Norberg, O., Pissarenko, N., & Barabash, S. W. (1991). On the momentum transfer of the solar wind to the Martian topside ionosphere. *Geophysical Research Letters*, *18*(6), 1059–1062. https://doi.org/10.1029/90GL02604

Ma, Y. J., Fang, X., Nagy, A. F., Russell, C. T., & Toth, G. (2014). Martian ionospheric responses to dynamic pressure enhancements in the solar wind. *Journal of Geophysical Research: Space Physics*, *119*(2), 1272–1286. https://doi.org/10.1002/2013JA019402

Mazelle, C., Winterhalter, D., Sauer, K., Trotignon, J., Acuña, M., Baumgärtel, K., et al. (2004). Bow shock and upstream phenomena at Mars. *Space Science Reviews*, *111*(1/2), 115–181. https://doi.org/10.1023/B:SPAC.0000032717.98679.d0

Mitchell, D. L., Mazelle, C., Sauvaud, J.-A., Thocaven, J.-J., Rouzaud, J., Fedorov, A., et al. (2016). The MAVEN solar wind electron analyzer. *Space Science Reviews*, *200*(1–4), 495–528. https://doi.org/10.1007/s11214-015-0232-1

Nagy, A. F., Winterhalter, D., Sauer, K., Cravens, T., Brecht, S., Mazelle, C., et al. (2004). The plasma environment of Mars. *Space Science Reviews*, *111*(1/2), 33–114. https://doi.org/10.1023/B:SPAC.0000032718.47512.92

Ramstad, R., Brain, D. A., Dong, Y., Espley, J., Halekas, J., & Jakosky, B. (2020). The global current systems of the Martian induced magnetosphere. *Nature Astronomy*, *4*(10), 979–985. https://doi.org/10.1038/s41550-020-1099-y

Riedler, W., Schwingenschuh, K., Lichtenegger, H., Möhlmann, D., Rustenbach, J., Yeroshenko, Y., et al. (1991). Interaction of the solar wind the planet Mars: Phobos 2 magnetic field observations. *Planetary and Space Science*, *39*(1–2), 75–81. https://doi.org/10.1016/0032-0633(91)90129-X

Romanelli, N., DiBraccio, G., Modolo, R., Leblanc, F., Espley, J., Gruesbeck, J., et al. (2019). Recovery timescales of the dayside Martian magnetosphere to IMF variability. *Geophysical Research Letters*, *46*(20), 10977–10986. https://doi.org/10.1029/2019GL084151

Romanelli, N., Modolo, R., Leblanc, F., Chaufray, J.-Y., Hess, S., Brain, D., et al. (2018). Effects of the crustal magnetic fields and changes in the IMF orientation on the magnetosphere of Mars: MAVEN observations and LatHyS results. *Journal of Geophysical Research: Space Physics*, *123*(7), 5315–5333. https://doi.org/10.1029/2017JA025155

Slavin, J. A., Acuña, M. H., Anderson, B. J., Barabash, S., Benna, M., Boardsen, S. A., et al. (2009). MESSENGER and Venus Express observations of the solar wind interaction with Venus. *Geophysical Research Letters*, *36*(9), L09106. https://doi.org/10.1029/2009GL037876

Trotignon, J., Mazelle, C., Bertucci, C., & Acuña, M. (2006). Martian shock and magnetic pile-up boundary positions and shapes determined from the Phobos 2 and Mars Global Surveyor data sets. *Planetary and Space Science*, *54*(4), 357–369. https://doi.org/10.1016/j.pss.2006.01.003

Wan, W. X., Wang, C., Li, C. L., & Wei, Y. (2020). China's first mission to Mars. *Nature Astronomy*, *4*(7), 721. https://doi.org/10.1038/s41550-020-1148-6

Wang, G. Q., Xiao, S. D., Wu, M. Y., Zhao, Y. D., Jiang, S., Pan, Z. H., et al. (2024). Calibration of the zero offset of the fluxgate magnetometer on board the Tianwen-1 orbiter in the Martian magnetosheath. *Journal of Geophysical Research: Space Physics*, *129*(1), e2023JA031757. https://doi.org/10.1029/2023JA031757

Wang, Y., Zhang, T., Wang, G., Xiao, S., Zou, Z., Cheng, L., et al. (2023). The Mars orbiter magnetometer of Tianwen-1: In-flight performance and first science results. *Earth and Planetary Physics*, *7*(2), 1–13. https://doi.org/10.26464/epp2023028

Wang, Z., Fu, H. S., Liu, C. M., Liu, Y. Y., Cozzani, G., Giles, B. L., et al. (2019). Electron distribution functions around a reconnection X-line resolved by the FOTE method. *Geophysical Research Letters*, *46*(3), 1195–1204. https://doi.org/10.1029/2018GL081708

Wang, Z., Fu, H. S., Vaivads, A., Burch, J. L., Yu, Y., & Cao, J. B. (2020). Monitoring the spatio-temporal evolution of a reconnection X-line in space. *The Astrophysical Journal Letters*, *899*(2), L34. https://doi.org/10.3847/2041-8213/abad2c

Wang, Z., Liu, X. Y., Fu, H. S., Cao, J. B., Dai, L., Toledo-Redondo, S., et al. (2024). First observation of kinetic Alfvén waves behind reconnection front in terrestrial magnetotail. *The Astrophysical Journal*, *960*(1), 45. https://doi.org/10.3847/1538-4357/ad0cb5

Xu, S., Mitchell, D. L., Weber, T., Brain, D. A., Luhmann, J. G., Dong, C., et al. (2020). Characterizing Mars's magnetotail topology with respect to the upstream interplanetary magnetic fields. *Journal of Geophysical Research: Space Physics*, *125*(3), e2019JA027755. https://doi.org/10.1029/2019JA027755

Xu, Y., Fu, H., Cao, J., Liu, C., Norgren, C., & Chen, Z. (2021). Electron-scale measurements of antidipolarization front. *Geophysical Research Letters*, *48*(6), e2020GL092232. https://doi.org/10.1029/2020GL092232

Xu, Y., Fu, H. S., Norgren, C., Hwang, K.-J., & Liu, C. M. (2018). Formation of dipolarization fronts after current sheet thinning. *Physics of Plasmas*, *25*(7), 072123. https://doi.org/10.1063/1.5030200

Yeroshenko, Y., Riedler, W., Schwingenschuh, K. I., Luhmann, J. G., Ong, M., & Russell, C. T. (1990). The magnetotail of Mars: Phobos observations. *Geophysical Research Letters*, *17*(6), 885–888. https://doi.org/10.1029/GL017i006p00885

Yu, Y., Fu, H. S., Cao, J. B., Liu, Y. Y., & Wang, Z. (2022). Electron rolling-pin distribution inside magnetic hole. *The Astrophysical Journal*, *926*(2), 199. https://doi.org/10.3847/1538-4357/ac497a

Zhang, T. L., Schwingenschuh, K., Russell, C. T., & Luhmann, J. G. (1991). Asymmetries in the location of the Venus and Mars bow shock. *Geophysical Research Letters*, *18*(2), 127–129. https://doi.org/10.1029/90GL02723

Zhao, M. J., Fu, H. S., Liu, C. M., Chen, Z. Z., Xu, Y., Giles, B. L., & Burch, J. L. (2019). Energy range of electron rolling pin distribution behind dipolarization front. *Geophysical Research Letters*, *46*(5), 2390–2398. https://doi.org/10.1029/2019GL082100

Zou, Z., Wang, Y., Zhang, T., Wang, G., Xiao, S., Pan, Z., et al. (2023). In-flight calibration of the magnetometer on the Mars orbiter of Tianwen-1. *Science China Technological Sciences*, *66*(8), 2396–2405. https://doi.org/10.1007/s11431-023-2401-2